“© 2017 IEEE. Personal use of this material is permitted. Permission from IEEE must be obtained for all other uses, in any current or future media, including reprinting/republishing this material for advertising or promotional purposes, creating new collective works, for resale or redistribution to servers or lists, or reuse of any copyrighted component of this work in other works.”

An Innovative Control Strategy for a Hybrid Energy Storage System (HESS)

Li Sun, Nong Zhang, Mohamed Awadallah and Paul Walker
Centre for Green Energy and Vehicle Innovations
University of Technology, Sydney
NSW, Australia
clickler@gmail.com, Nong.zhang@uts.edu.au, Mohamed.M.Awadallah@student.uts.edu.au, Paul.walker@uts.edu.au

***Abstract*—Electric Vehicles (EVs) adopting both batteries and supercapacitors have attracted a significant amount of attention in research communities due to its unique power sharing capabilities. A Hybrid Energy Storage System (HESS) can effectively reduce power stress that would otherwise be applied to batteries alone, and whose weight and size is still a common concern when competing against conventional ICE-powered cars. In this paper, a high-level control strategy is developed to adaptively split the load between two sources for an electric vehicle adopting HESS under real-life load fluctuations. A converter – Supercapacitor Pack (SP) coupled HESS upon which such an algorithm is deployed on, is proposed to divert excess power that would otherwise overdraw from or damage the Battery Pack (BP) into the SP via a smart Power Converter (PC) which is located in between in order to regulate both behaviors. Such a power split strategy (PSS) is designed in such a way to track real-time load profiles and determines one important variable – the cut-off frequency. As a consequence, relatively higher frequency portion of the load power gets channeled to the SP and the remaining less-varying power demand is sent to the BP based on the fundamental energy balancing equation. A simplified HESS model is first developed. The power split algorithm is coded in Matlab and then applied to this HESS model. Finally, the overall system is tested comprehensively over 4 EPA driving cycles. Simulation results prove its effectiveness in coping with even the harshest driving scenarios in real life.**

Keywords—Li-ion Batteries; Supercapacitors; bidirectional DC-DC converters; energy management strategy; Discrete Fourier Transform (DFT)

NOMENCLATURE

BP	Battery Pack
DFT	Discrete Fourier Transform
EMS	Energy Management Strategy
ESS	Energy Storage System
FIR	Finite Impulse Response
HESS	Hybrid Energy Storage System
LPF	Low Pass Filter
PAPR	Peak-to-Average Power Ratio
PAPV	Peak-to-Average Velocity Ratio
PC	Power Converter
PSS	Power Split Strategy
SOC	State Of Charge
SP	Supercapacitor Pack

I. Introduction

Most existing electric vehicles employ rechargeable batteries alone. As a consequence, they suffer from performance degradation such as power deprivation or battery aging, and have difficulty to cope with the whole spectrum of driving load without compromising durability or safety [1]-[4].

To address these problems one obvious solution is to *oversize* the BP, similar to the Tesla® (U.S.) and BYD® (China) pure EVs. However doing so is sub-optimal as it induces a heavy penalty on overall system weight and cost.

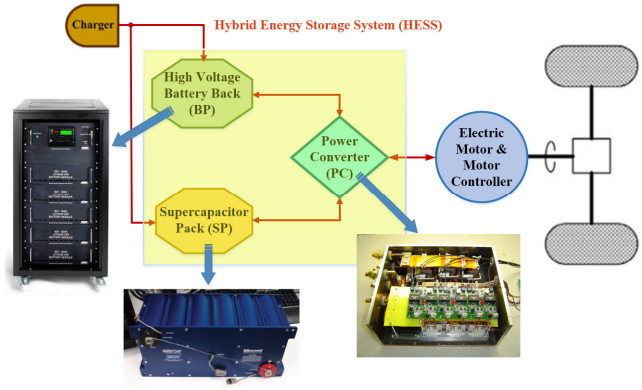

Fig. 1. The configuration of an active HESS equipped in an EV.

To solve this pain, concepts such as HESS have been proposed across various literatures [5]-[9], whose aim is to divert excess power, that would otherwise overdraw from or damage the BP to a dedicated power source such as an SP. In most cases, such coordination is achieved by introducing a smart power converter (PC) - a device located in between the BP and SP so as to regulate both behaviours. In practice, a bi-directional DC-DC converter is normally utilized as PC. Such a HESS is called an *active* HESS with its main components and power flow shown in Fig. 1.

Whilst the main focus of this paper is *not* on how to design a better topology, it is worth mentioning that, after a comprehensive study done by Schupbach and Balda in [8], they came to a conclusion that a half bridge buck-boost topology obtains most merits, from both performance and cost aspects, over some of the other topologies. We, therefore, decided to study and design EMS based on *this* conventional topology, with the aims to develop *better* algorithm to intelligently split load power between BP and SP *as a function of* the ever-changing load profile.

A considerable amount of research has been done in this field. For example, R. Carter, *et al* [10] proposed a method where a threshold is set beyond which the excess power demand is filled up by SP when permitted. Furthermore, J. Trovão, *et al* [11] have broken down the criteria – such as the SOC of BP or the SOC of SP – into four levels and organize them on a 2D map such that, by combining other rules on the load side, a much finer control can be accomplished. Moreover, Zhang, *et al* [12] proposed a fuzzy logic controller that accepts battery SOC,

supercapacitor SOC, and desired load power as inputs. Based on selected inputs and various contraints, the power split ratio is set. Another method is to design via load-leveling itself such as in [13][14]. Each individual component of similar hybridized systems can be optimized through such a process.

One particular control strategy of interest is the filter based control, where the idea (Fig. 2) is not difficult to grasp: by considering the *frequency spectrum* of the load profile in *retrospective*, a low pass filter or band pass filters can be applied to it so that lower frequency portion of the load (i.e. baseload) can be extracted and sourced from the BP. Research work [15]-[17] has been conducted and combining with other rules mentioned before, they worked relatively well, at least in the simulation environment.

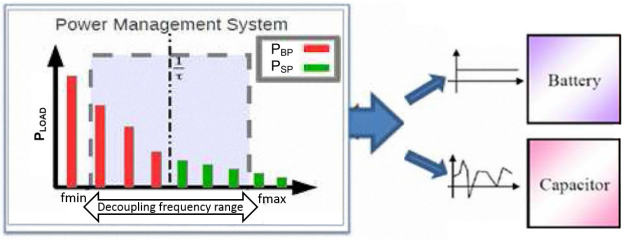

Fig. 2. Filter based RB control to address PSS problem[18].

One drawback of this approach, however, is that the cutoff frequencies of the filter designs are often kept as constants. H. Xiaoliang, *et al* [18] has expanded this limitation by introducing two frequency thresholds, one for urban, the other for highway, and dynamically switches them over on-the-fly. This greatly increases effectiveness of the PSS algorithm however, a proper timing signal is needed for the supervisory system to determine which drive pattern is the vehicle currently operating on.

This paper attempts to resolve this issue, and is arranged as follows: in Section II, the frequency-adaptive PSS algorithm is developed. The proposed PSS is then first coded in Matlab where it was tested rigorously across 4 mainstream driving cycles in Section III. Analysis is conducted afterwards also in Section III to gain insights into evaluating how useful is such PSS. Conclusions are drawn in section VI.

II. Frequency-Adaptive PSS – Algorithm Development

A. Overall HESS Layout and Power Flow Analysis

In this study, a interleaved half-bridge DC-DC converter [38] is adopted. It is worth mentioning that the *Zero Voltage Switching* (ZVS) technique developed in [19] and applied in this work has greatly reduced the switching loss of the converter and thereby boosts its overall efficiency at around 98% under full load condition. Such evidences have greatly offset the downside of putting the SP at the low voltage side of the converter while reducing overall system heat dissipation. The device's stress can also be greatly alleviated by using such a technique, and hence the total lifecycle of the converter is increased.

The overall HESS system is shown in Fig. 3, and it can be understood based on the fundamental Kirchhoff's current law (KCL). The output current of the SP, i.e. I_{SP} is restricted and bundled with the PC. By actively controlling I_{SP}, we could indirectly regulate the current from the BP, i.e. I_{BP} simultaneously, at any given load current, i.e. I_{LOAD}. Since Vdc is tightly clamped by a relatively *stiff* voltage source – BP, regulating I_{SP} *alone* is sufficient to influence power split.

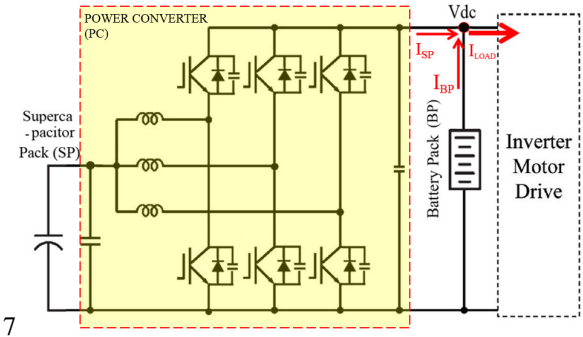

Fig. 3. Overall HESS layout and node analysis at Vdc.

In essence, when KCL is applied on node Vdc in Fig. 3, we get:

$$I_{LOAD} = I_{SP} + I_{BP} \quad (1)$$

Note that the *load* is caused by an inverter motor drive unit. This control approach is bi-directional so the arrows, as shown in Fig. 7, can be reversed as well. For example, the arrows of I_{LOAD} reverses when the EV is running under regenerative braking.

B. Algorithm Development

In order to *adaptively* extract this slow-moving, i.e. lower frequency portion of I_{LOAD}, we adopted an "adaptive filter". An adaptive filter is a filter that self-adjusts its transfer function according to requirements, in our case, the load. However, such techniques are generally computationally expensive and sometimes, cause non-converging [20]. In our work, a simplified adaptive digital LPF structure is proposed that is guaranteed to converge and is practical to implement. The complete flowchart of proposed PSS is shown in Fig. 4 (Patent pending).

In general, the algorithm runs on two loops, the main/outer loop iterates in sync with real-time. The inner loop determines, within one main-loop cycle, the *instantaneous* cut-off frequency based on a length of historic data that also gets updated every main-loop cycle.

More specifically, it starts by setting two variables, *w*, for *window length* upon which subsequent DFT [21] applies, the other is *R*, which stands for the *ratio of area* (under the frequency spectrum plot), whose job is to locate the instantaneous cut-off frequency.

Current sensor is first deployed to measure I_{LOAD}, DFT is then applied to the most recent *w* length of $\vec{I}_{LOAD}$. Another vector $\vec{I}_{LOAD\_f}$ is obtained as output, whose elements are all *complex numbers*. The inner loop is then kicked in to determine the location of the cut-off frequency for the *current* loop cycle, based on one criterion:

$$AREA \geq R * \int_0^{+\infty} \left| \vec{I}_{LOAD\_f} \right| df = R * \sum \left| \vec{I}_{LOAD\_f} \right| \quad (2)$$

where AREA is literally the *integral*, or in discrete domain, the sum of values of each column in *red* as shown in Fig. 2 that is unknown, and $\sum |\vec{I}_{LOAD\_f}|$ is the sum of values of all columns in both *red* and *green*. Note that modulus operation is performed to extract *meaningful* contents of each element. Obviously R must be chosen as equal or less than unity.

Once R is set, the inner loop breaks out whenever (2) is met and the most recent *j* is retrieved and used as *another*

index to calculate the instantaneous cut-off frequency *f_c(i)* at the current time.

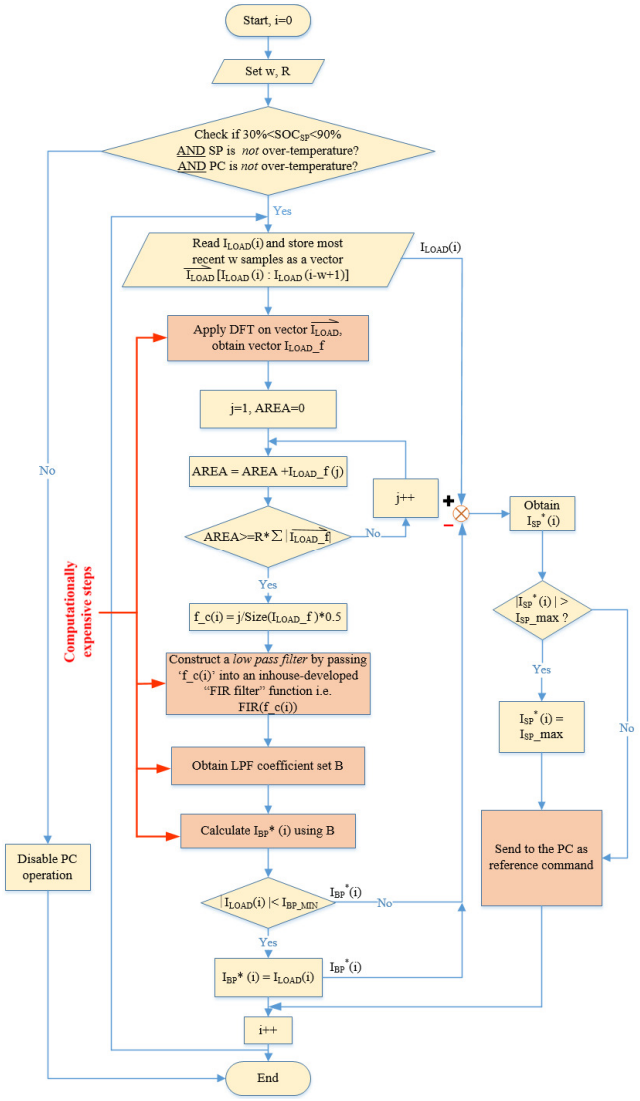

Fig. 4. Flowchart of frequency adaptive PSS algorithm (Patent pending).

Considering the nature of any digital IIR(Infinite Impulse Response) filters may generate an unstable response[21], and an FIR filter is used to construct a LPF that is guranteed to be always stable. By specifying other parameters such as "Passband frequency", "Stopband frequency", "Passband ripple", "Stopband attenuation", as well as *f_c(i),* in either Matlab[22], the LPF coefficients set B can be obtained. Consequently, $I_{BP}^*(i)$ can be obtained when passing I_{LOAD} through B. This output $I_{BP}^*(i)$, serves a pivotal *meaning* in the whole framework as the *reference operating point* the BP to be *ideally* operated at. From (1), $I_{SP}^*(i)$ can then be calculated and sent to PC as reference command.

In practice, in order to avoid frequent turn-on-and-off event for the PC, especially under light load conditions, we further restrict $I_{BP}^*(i)$ to follow the *exact* I_{LOAD} profile when I_{LOAD} is below certain threshold $I_{BP\text{-}MIN}$, as shown at the bottom of the flowchart in Fig. 4.

III. PSS Evaluation over 4 Driving Cycles

A. Load Power Analysis and Assumptions

In order to evaluate the overall performance of the PSS, we adopted a practical EV model in our assessment with its key characteristics assumed in Table I. In addition, four EPA driving cycles [23] were carefully chosen to emulate load. In it, tyre rolling resistance F_r can be calcluated using (3), and aerodynamic drag F_d can be calculated using (4).

$$F_r = C_r Mg \quad (3)$$

$$Fa = 0.5\rho A C_d V^2 \quad (4)$$

TABLE I
KEY CHARACTERISTICS OF A PASSENGER EV

Symbol	EV characteristic (Unit)	Value
M	Vehicle mass (kg)	1460
C_r	Aerodynamic drag coefficient (-)	0.28
A	Frontal area (m^2)	2.2
ρ	Air density (kg/m^3)	1.29
C_d	Rolling resistance coefficient (-)	0.016
R_w	Wheel radius (m)	0.2794
V	Vehicle velocity	Downloadable from [23]

Note that in this simulation, minor parasitic terms such as equivalent mass factor are neglected. A further simplification is made below.

1) The electrical energy conversion effeciency (η) is assumed at a fixed 90%, across all 4 driving cycles.
2) The vehicle is driving on a perfectly flat road (i.e. zero grade).

TABLE II
KEY CHARACTERISTICS/PARAMETERS OF DRIVING CYCLES FOR AN EV CHARACTERIZED IN TABLE I (AT ZERO GRADE)

	NEDC	UDDS	US06	LA92
Distance (m)	10932	11990	12885	15797
Duration (s)	1184	1369	598	1435
Peak velocity (km/hr)	120	90.7	129.2	108.1
Average velocity (km/hr)	33.2	31.5	76.9	43.3
PAVR (-)	3.61	2.88	1.68	2.50
Maximum acceleration (m/s^2)	1.04	1.47	3.24	2.82
Maximum deceleration (m/s^2)	-0.98	-1.47	-2.82	-3.75
Peak acceleration power (kW)	35.32	32.25	70.83	43.57
Average acceleration power (kW)	7.59	6.84	20.73	10.86
PAPR (acceleration) (-)	4.65	4.71	3.42	4.01
Peak deceleration power (kW)	-25.25	-22.67	-43.66	-73.73
Average deceleration power (kW)	-6.41	-6.42	-15.77	-9.45
PAPR (deceleration) (-)	3.94	3.53	2.76	7.80
PAPR/PAVR (acceleration) (-)	1.29	1.64	2.04	1.60
PAPR/PAVR (deceleration) (-)	1.09	1.23	1.64	3.12
Intermediate stops	13	15	4	14

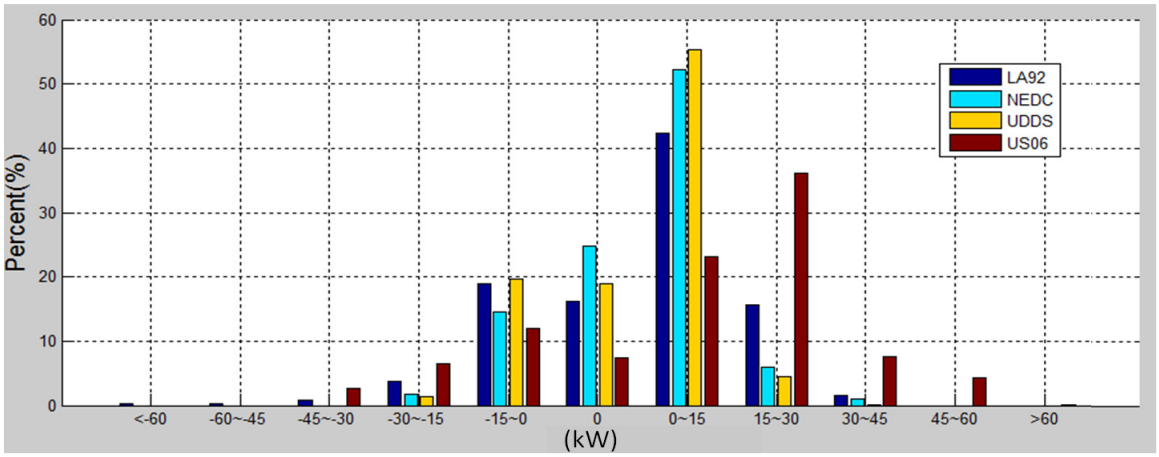

Fig.5. Comparison for load power histogram amongst all four driving cycles in evaluation.

Therefore, combined with the velocity profiles downloaded from [23] for the chosen 4 driving cycles, the overall load parameters, including load resistance or power P_{LOAD}, can be calculated using (5) and are summarized in Table II.

$$P_{LOAD} = (V/\eta)*[Ma+F_r+Fa] \quad (5)$$

where a is the vehicle acceleration. A detailed broken-down analysis was then conducted to better compare load power characteristics across all four driving cycles in Fig. 5.

Note that our objective is to choose driving cycles in order to cover as wide a spectrum of the velocity and the power profiles, as possible.

Based on Table II and Fig. 5, these four driving cycles were chosen for the following reasons:

1) Amongst all 4 driving cycles, the US06 possesses the highest peak velocity and most aggressive driving characteristics during *acceleration*.
2) Amongst all 4 driving cycles, the LA92 presents the most aggressive driving characteristics during *deceleration*.
3) The NEDC has the mildest characteristics across all 4 cycles, as it obtains *lowest* maximum acceleration and deceleration amongst all 4 driving cycles. Therefore, it is chosen as a *baseline* for other cycles to compare against.
4) The UDDS has the highest number count for intermediate stops, in Table II, and is used to test the PSS in stop-and-go events. The well-known New York City Cycle (NYCC) [23] is not chosen in this study, because its top speed is too low.
5) The also-well-known Highway Fuel Economy Driving Schedule (HWFET) [23] is not used here either, because there is little transient or dynamic needs for PSS to function in *steady* high way driving. Let alone, a substantial portion of the US06 is representative enough to address the high-way driving pattern as shown in Fig. 8.)

In order to quantify the level of the overall load fluctuation, L. Sun and N. Zhang [24] proposed using one simple metric – PAPR. However, one drawback of using the PAPR alone is that if, throughout the whole driving cycle, the occurance of the "relatively *high* load power region" is *infrequent* (e.g. in the NEDC it only occurs *once* after 1,000th second as shown in Fig. 6; In the UDDS as well, it only occurs *once* between 200th second and 300th second as shown in Fig. 7), then using PAPR alone is somewhat misleading as it reflects *less* of the degree of the *overall* load fluctuation.

To compensate, in this paper, we normalized PAPR by *dividing it against* PAVR, with the aims to reflect *closer* the level of the *overall* load fluctation. As can be seen in Table II, excluding the zero-power (or zero-velocity) regions in all driving cycles, the UDDS, US06 and LA92 present a significantly higher PAPR/PAVR value than that of the NEDC during acceleration. Whereas during deceleration, PAPR/PAVR value of the LA92 almost *triples* that of the NEDC. The needs to alleviate such excessive stress becomes obvious in even, driving cycles stipulated by U.S. government.

B. Simulation Results and Comparison

In order to evaluate the proposed PSS developed in II-B, simulation is conducted on the EV characterized in Table I, across all 4 driving cycles as described in III-A. The results are plotted from Fig. 6-9 (w=50, R=0.3 is chosen in the simulation).

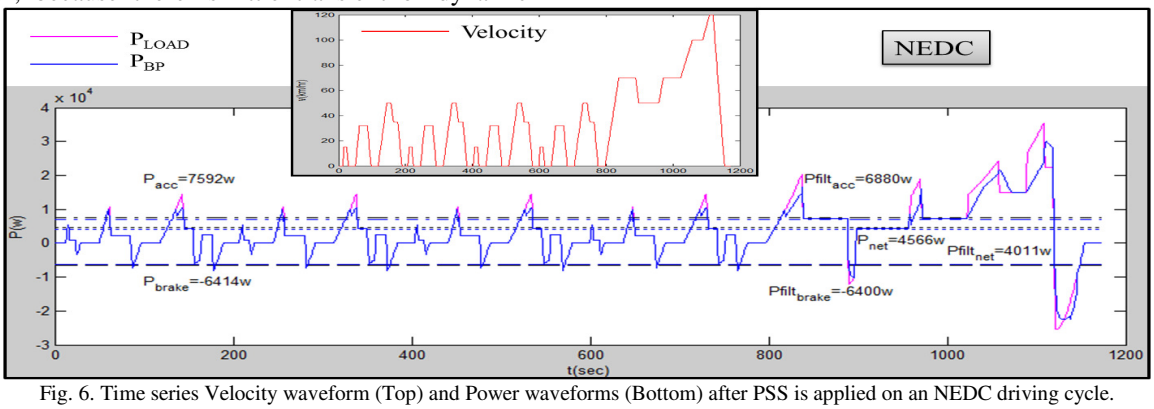

Fig. 6. Time series Velocity waveform (Top) and Power waveforms (Bottom) after PSS is applied on an NEDC driving cycle.

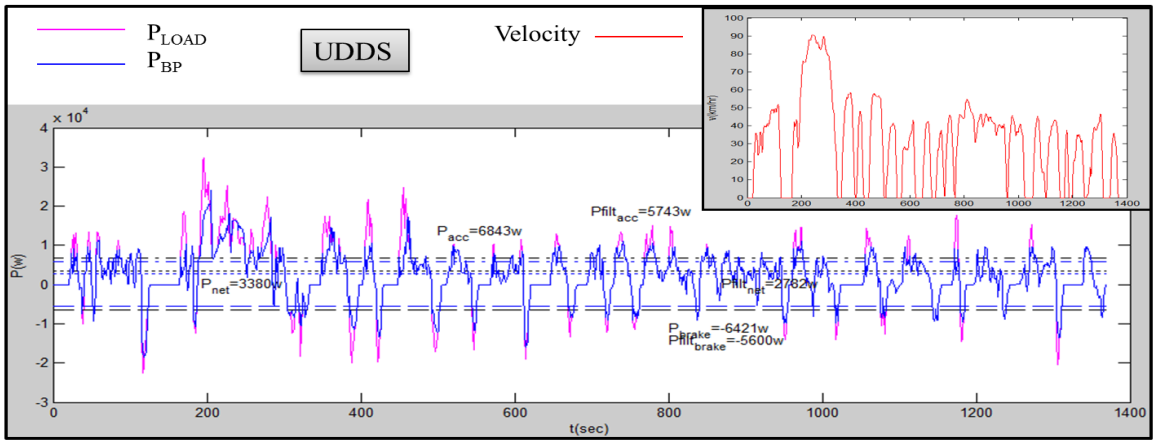

Fig. 7. Time series Velocity waveform (Top) and Power waveforms (Bottom) after PSS is applied on a UDDS driving cycle.

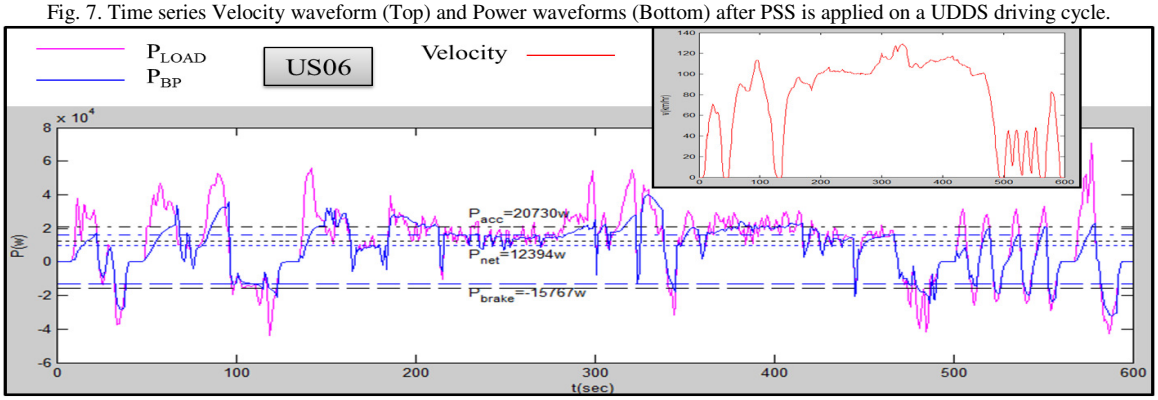

Fig. 8. Time series Velocity waveform (Top) and Power waveforms (Bottom) after PSS is applied on a US06 driving cycle.

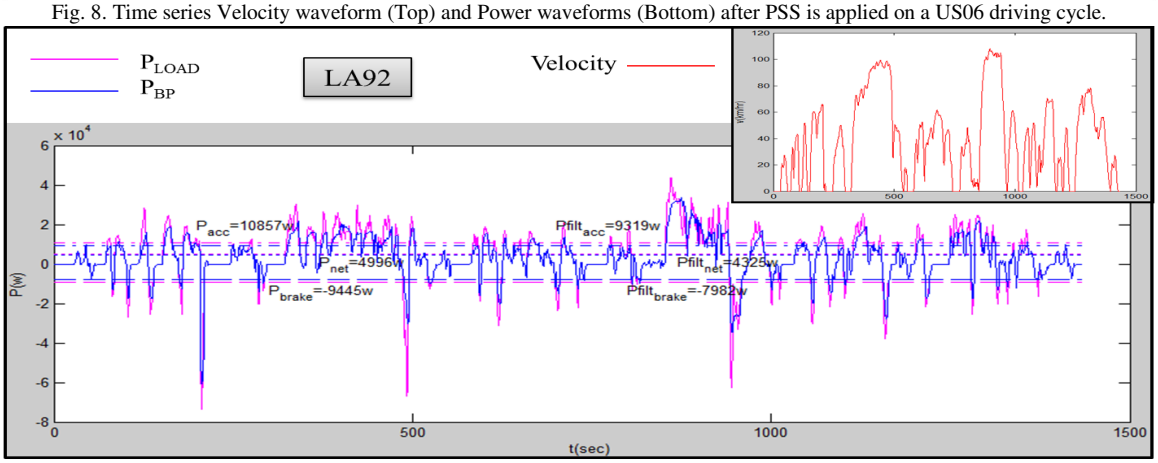

Fig. 9. Time series Velocity waveform (Top) and Power waveforms (Bottom) after PSS is applied on an LA92 driving cycle.

Note that since Vdc (in Fig. 3) is unspecified in this simulation, instead of I_{LOAD} and I_{BP}, P_{LOAD} and P_{BP} are calculated and plotted.

In addition, in order to avoid frequent turn-on-and-off event for the PC, P_{BP} is restricted to follow the *exact* P_{LOAD} profile when P_{LOAD} is between +10kW and -10kW. Two comparisons are conducted in order to evaluate the overall effectiveness of the PSS during acceleration and deceleration each respectively. We use the *percentage of the PAPR/PAVR reduction* before and after deploying the PSS, to determine the effectiveness of the algorithm. The results are summarized in Table III and IV.

A few observations are reported below:

1) During acceleration, the proposed PSS works *best* for the US06 driving cycle, which is characterized as the most aggressive driving cycle amongst all 4 test driving cycles. Moreover, its effectiveness *proportionally* decreases as the value of PAPR/PAVR reduces over all 4 test driving cycles. This makes sense as there is little need to perform load-leveling for the mildest NEDC driving cycle.

TABLE III
A BP-ONLY ESS WITHOUT PSS APPLIED (BEFORE) V.S. AN HESS WITH THE PROPOSED PSS APPLIED (AFTER) (DURING ACCELERATION).

Driving Cycle	Peak acceleration Power (kW)		Average acceleration Power (kW)		PAPR (acceleration)		PAVR	PAPR/PAVR (acceleration)		**PAPR/PAVR Reduction (%)**
	Before	After	Before	After	Before	After		Before	After	
NEDC	35.32	29.96	7.59	6.88	4.65	4.35	3.61	1.29	1.21	**-6.4%**
UDDS	32.25	23.97	6.84	5.74	4.71	4.18	2.88	1.64	1.45	**-11.3%**
US06	70.83	40.17	20.73	16.3	3.42	2.46	1.68	2.04	1.47	**-27.9%**
LA92	43.57	33.73	10.86	9.32	4.01	3.62	2.50	1.60	1.45	**-9.7%**

TABLE IV
A BP-ONLY ESS WITHOUT PSS APPLIED (BEFORE) V.S. AN HESS WITH THE PROPOSED PSS APPLIED (AFTER) (DURING REGENERATIVE BRAKING).

Driving	Peak deceleration Power (kW)		Average deceleration Power (kW)		PAPR (deceleration)		PAVR	PAPR/PAVR (deceleration)		**PAPR/PAVR Reduction**
Cycle	Before	After	Before	After	Before	After		Before	After	**(%)**
NEDC	-25.25	-22.56	-6.41	-6.4	3.94	3.53	3.61	1.09	0.98	**-10.5%**
UDDS	-22.67	-18.58	-6.42	-5.6	3.53	3.32	2.88	1.23	1.15	**-6.0%**
US06	-43.66	-31.68	-15.77	-12.96	2.76	2.44	1.68	1.64	1.46	**-11.4%**
LA92	-73.73	-60.89	-9.45	-7.98	7.8	7.63	2.50	3.12	3.05	**-2.2%**

2) During deceleration, the algorithm works best for the US06 driving cycle as well. However, for driving cycles contain a large amount of *abrupt* deceleration events, such as the UDDS and the LA92, the effectiveness of the PSS reduces.
3) As shown in Fig. 8, a clear *smoothening* effect can be spotted duing the high-way cruising portion of the US06. The adaptive filter follows the trend of the load especially well within this period.

Finally, it is worth mentioning that, although it is desirable to reduce the value of PAPR/PAVR within a driving cycle, there are limitations that the PC and SP may fail supporting the diverted load. Therefore, careful matching and control may be needed to intervene in practice.

IV. CONCLUSIONS

In this paper, an innovative adpative PSS has been proposed and simulated on a battery-supercapacitor EV powertrain. Design principles of the control strategy are specified in this paper. Comprehensive driving cycle simulation discloses a positive correlation between the effectiveness of the proposed PSS and the value of PAPR/PAVR for all four test driving cycles during acceleration. Furthermore, effectiveness of the PSS reduces for driving cycles containing many abrupt deceleration events.

Although we specifically present the results for HESS applications, the concept of both HESS and PSS can be easily tailored for other types of hybridized systems such as *series hybrid electric vehicles*, *battery assisted fuel cell electric vehicles*, *solar-battery power systems* or any *dual-source power systems* that need to perform load-leveling functions.

REFERENCES

[1] D. B. Edwards and C. Kinney, “Advanced lead acid battery designs for hybrid electric vehicles,” in Proc. 16th Battery Conf. Appl. Adv.,Jan. 2001, pp. 207–212.

[2] M. C. Wehrey, “What’s new with hybrid electric vehicles,” IEEE PowerEnergy Mag., vol. 2, no. 6, pp. 34–39, Nov./Dec. 2004.

[3] E. Karden, S. Ploumen, B. Fricke, T. Miller, and K. Snyder, “Energy storage devices for future hybrid electric vehicles,” J. Power Sources, vol. 168, no. 1, pp. 2–11, May 2007.

[4] Omar, N., et al. (2014). "Lithium iron phosphate based battery - Assessment of the aging parameters and development of cycle life model", Applied Energy, Volume 113, January 2014, Pages 1575-1585.

[5] S. Pay and Y. Baghzouz, "Effectiveness of battery-supercapacitor combination in electric vehicles," in Power Tech Conference Proceedings, 2003 IEEE Bologna, 2003, p. 6 pp. Vol.3.

[6] A. Khaligh, A. Miraoui, and D. Garret, “Guest editorial: Special section on vehicular energy-storage systems,” IEEE Trans. Veh. Technol., vol. 58, no. 8, pp. 3879–3881, Oct. 2009.

[7] J. Cao and A. Emadi, "A New Battery/UltraCapacitor Hybrid Energy Storage System for Electric, Hybrid, and Plug-In Hybrid Electric Vehicles," Power Electronics, IEEE Transactions on, vol. 27, pp. 122-132, 2012.

[8] Schupbach, R.M.; Balda, J.c.;"Comparing DC-DC converters for power management in hybrid electric vehicles", IEMDC' 03. IEEE International , vol.3, pp. 1369- 1374 , June 2003.

[9] S. Lu, K. A. Corzine, and M. Ferdowsi, "A New Battery/Ultracapacitor Energy Storage System Design and Its Motor Drive Integration for Hybrid Electric Vehicles," Vehicular Technology, IEEE Transactions on, vol. 56, pp. 1516-1523, 2007.

[10] R. Carter, A. Cruden and P. J. Hall, "Optimizing for Efficiency or Battery Life in a Battery/Supercapacitor Electric Vehicle," in *IEEE Transactions on Vehicular Technology*, vol. 61, no. 4, pp. 1526-1533, May 2012.

[11] João P. Trovão, Paulo G. Pereirinha, Humberto M. Jorge, Carlos Henggeler Antunes, *A multi-level energy management system for multi-source electric vehicles – An integrated rule-based meta-heuristic approach*, Applied Energy, Volume 105, May 2013, Pages 304-318, ISSN 0306-2619

[12] Zhang Chenghui; Shi Qingsheng; Cui Naxin; Li Wuhua, Particle Swarm Optimization for energy management fuzzy controller design in dual-source electric vehicle, in Power Electronics Specialists Conference, 2007. PESC 2007. IEEE , vol., no., pp.1405-1410, 17-21 June 2007

[13] Baumann BM, et al. Mechatronic design and control of hybrid electric vehicles. Mechatronics, IEEE/ASME Transactions on 2000;5(1):58–72.

[14] Schouten NJ, Salman MA, Kheir NA. Fuzzy logic control for parallel hybrid vehicles. Control Systems Technology, IEEE Transactions on 2002;10(3):460–8.

[15] Jaafar, A.; Akli, C.R.; Sareni, B.; Roboam, X.; Jeunesse, A., Sizing and Energy Management of a Hybrid Locomotive Based on Flywheel and Accumulators," in Vehicular Technology, IEEE Transactions on , vol.58, no.8, pp.3947-3958, Oct. 2009

[16] Schaltz, E.; Khaligh, A.; Rasmussen, P.O., *Influence of Battery/Ultracapacitor Energy-Storage Sizing on Battery Lifetime in a Fuel Cell Hybrid Electric Vehicle*, in Vehicular Technology, IEEE Transactions on , vol.58, no.8, pp.3882-3891, Oct. 2009

[17] Ravey, A.; Roche, R.; Blunier, B.; Miraoui, A., *Combined optimal sizing and energy management of hybrid electric vehicles*, in Transportation Electrification Conference and Expo (ITEC), 2012 IEEE , vol., no., pp.1-6, 18-20 June 2012

[18] H. Xiaoliang, T. Hiramatsu and H. Yoichi, "Energy Management Strategy based on frequency-varying filter for the battery supercapacitor hybrid system of Electric Vehicles," Electric Vehicle Symposium and Exhibition (EVS27), 2013 World, Barcelona, 2013, pp. 1-6.

[19] Junhong Zhang; Jih-Sheng Lai; Rae-young Kim; Wensong Yu, "High-Power Density Design of a Soft-Switching High-Power Bidirectional dc–dc Converter," *Power Electronics, IEEE Transactions on* , vol.22, no.4, pp.1145,1153, July 2007

[20] Rupp, Markus. "Adaptive filters: stable but divergent." EURASIP Journal on Advances in Signal Processing 2015.1 (2015): 1.

[21] A. Oppenheim and R. W. Schafer, Discrete-Time Signal Processing, Pearson, 2009

[22] V. Ingle and J. Proakis, ‘Digital Signal Processing using Matlab’, Cengage Learning, 2012

[23] "Dynamometer Drive Schedules", [online]. Available: https://www.epa.gov/vehicle-and-fuel-emissions-testing/dynamometer-drive-schedules (Accessed 20 Aug 2016).

[24] L. Sun and N. Zhang, "Reducing the Peak-to-average Power Ratio for Electric Vehicles using Hybrid Energy Storage Systems (HESS)", Electric Vehicle Symposium and Exhibition (EVS29), Montreal, 2016.